

Spiral-like structure at the centre of nearby clusters of galaxies

T. F. Laganá¹, F. Andrade-Santos¹, and G. B. Lima Neto¹

Universidade de São Paulo, Instituto de Astronomia, Geofísica e Ciências Atmosféricas, Departamento de Astronomia, Rua do Matão 1226, Cidade Universitária, 05508-090, São Paulo, SP, Brazil.

Received 26 August 2009 / Accepted 17 November 2009

ABSTRACT

Context. X-ray data analysis have found that fairly complex structures at cluster centres are more common than expected. Many of these structures have similar morphologies, which exhibit spiral-like substructure.

Aims. It is not yet well known how these structures formed or are maintained. Understanding the origin of these spiral-like features at the centre of some clusters is the major motivation behind this work.

Methods. We analyse deep *Chandra* observations of 15 nearby galaxy clusters ($0.01 < z < 0.06$), and use X-ray temperature and substructure maps to detect small features at the cores of the clusters.

Results. We detect spiral-like features at the centre of 7 clusters: A85, A426, A496, Hydra A cluster, Centaurus, Ophiuchus, and A4059. These patterns are similar to those found in numerical hydrodynamic simulations of cluster mergers with non-zero impact parameter. In some clusters of our sample, a strong radio source also occupies the inner region of the cluster, which indicates a possible connection between the two. Our investigation implies that these spiral-like structures may be caused by off-axis minor mergers. Since these features occur in regions of high density, they may confine radio emission from the central galaxy producing, in some cases, unusual radio morphology.

Key words. Keywords should be given

1. Introduction

Previous studies have shown that many clusters continue to be in the process of forming, groups or individual galaxies being accreted from the outer large scale structure filaments (e.g., Durret et al. 2003). Temperature maps of the X-ray emitting gas have shown that even clusters with apparently relaxed structures in X-ray can have perturbed temperature maps, which are indicative of recent ongoing mergers (e.g., Finoguenov et al. 2005; Durret & Lima Neto 2008). The detection of these small structures is one of the main achievements of the present era of X-ray telescopes such as *Chandra* and *XMM-Newton*. However, the presence of cooling cores suggest that recent merger(s) have not had enough time to destroy the cooling core.

More than 70% of cooling-flow clusters contain a central cD galaxy that is a radio source (e.g., Burns 1990; Eilek 2004). *Chandra* observations of these systems found that the core of many clusters exhibit morphological complexities that are probably produced by the interaction between the intracluster medium (ICM) and the central radio galaxy.

The most important connection between the X-ray ICM and the non-thermal relativistic electrons that pro-

duce radio emission is dynamical. In the case of very energetic jets, the ICM is heated and compressed because of supersonic shocks (Heinz et al. 1998; Reynolds et al. 2001). However, there are weaker jets that do not provide an efficient shock heating, but instead a bubble of low-density gas, which can be identified as a depression in the X-ray surface brightness, that rises because of buoyancy (e.g., Churazov et al. 2001; Brüggén & Kaiser 2002; McNamara et al. 2005).

On the other hand, the ICM can also affect the radio emission from radio galaxies by placing upper limits on the radio emission. The unusual radio morphology of central cluster galaxies that fill X-ray cavities of low density has been reported previously (Boehringer et al. 1993; Taylor et al. 1994; Fabian et al. 2000, 2002; Taylor et al. 2002). The most extreme case of radio distortion is the amorphous radio galaxy PKS 0745-191 at the core of the Centaurus cluster (Taylor et al. 1994).

Another interesting feature is the spiral-like feature at the core of Perseus (Churazov et al. 2003; Fabian et al. 2000; Taylor et al. 2002), A2204 (Sanders & Fabian 2008), and A2029 (Clarke et al. 2004). This spiral pattern was also found in hydrodynamical simulations of merging clusters with non-zero impact parameters (Gómez et al. 2002;

Ascasibar & Markevitch 2006). In these simulations, the infalling sub-cluster causes a disturbance in the mass peak as it passes through the cluster centre. Thus, the central cool gas of the main cluster acquires angular momentum, producing its spiral pattern.

To understand more clearly the ICM-radio interaction and to characterize the spiral feature, we present a sample of 15 nearby clusters, among which 7 exhibit this feature in temperature and substructure maps, and a large cooling-flow and an embedded radio galaxy at the centre. The paper is organized as follows: in Sect. 2, we describe the data sample and the *Chandra* data analysis; in Sect. 3, we explain the image procedures used to detect the spiral-like pattern; in Sect. 4, we present our results and notes for individual clusters; in Sect. 5, we discuss a possible scenario to explain the spiral-like feature formation and the ICM-radio connection; in Sect. 6, we present a synthetic image produced to reproduce the surface brightness of the Perseus cluster, and in Sect. 7, we summarize our findings.

All distance-dependent quantities are derived by assuming the Hubble constant $H_0 = 70 \text{ km s}^{-1} \text{ Mpc}^{-1}$, $\Omega_M = 0.3$ and, $\Omega_\Lambda = 0.7$.

2. Observation and data reduction

2.1. Cluster selection

The objects in our sample were selected from a set of clusters within the redshift range $0.01 < z < 0.06$ with *Chandra* public data. We imposed that the data for each cluster had a long exposure time, that is, of at least 35 ks. Our final sample contained 15 clusters, whose properties are presented in Tab. 1.

2.2. Chandra data reduction

To obtain calibrated images without artifacts, that are adequate for achieving our goals, it is necessary to follow a series of procedures, otherwise we would have contamination, which can be detected as substructures.

We used the package CIAO 3.4. A level 2 event file was initially generated from a level 1 event file, using the standard procedure¹ and the latest calibration of CALDB 3.3.0. Periods with flares, which are spurious high counts caused by protons accelerated by the Sun, were excluded using the *lc_clean* script. At this point, a rebinned image with pixels corresponding to 16 raw physical pixels (4x4) was created from the new level 2 event file, in the energy band from 0.3 to 7.0 keV. We then produced exposure maps and used them to obtain flat images from which the source points were removed by filling circles around each source by randomly sampling the same distribution as found in a circular region close to the source. Finally, we fitted a 2D analytical surface brightness model.

3. Imaging

Since the bremsstrahlung emissivity depends on both the temperature and surface brightness, irregularities can be detected either in terms of temperature or density discontinuities. Since $\epsilon \propto T^{1/2} n^2$, these substructures are more significant in the surface brightness maps. Thus, to resolve the degeneracy, we used substructure (which depends on the surface brightness distribution, ?) and temperature maps to analyse in detail the inner parts of the clusters in our sample. of significant structure in the inner region of several clusters. To investigate this further, we compared these images with the temperature and the substructure maps.

3.1. X-ray substructures

We developed a new method to quantify substructures in clusters of galaxies using 2D surface brightness fits. This method was tested for 47 galaxy clusters observed with *Chandra* (?).

The method is based on analysing the number and intensity of substructures detected by a *friends-of-friends* (FOF) algorithm. This analysis is performed on a residual image, which is produced by fitting a bidimensional analytical model (β -model or Sérsic) with elliptical symmetry (using Sherpa/CIAO, which fits a model by minimizing the χ^2) to the cluster X-ray image. All surface brightness model parameters are free to vary, including the ellipticity, position angle, and centre. In particular, to identify substructures, we used a threshold in the residual image to separate the pixels that had counts statistically significantly above or below the 2D fitted model surface brightness at the corresponding position. The threshold was defined to be 3 times the local X-ray background variance. Once the pixels were separated, we identified these regions as substructures, using the FOF algorithm to link together the pixels above the threshold. This is a robust method if applied to high signal to noise ratio observations, which is the case, since the clusters in our sample are rich objects at very low redshifts ($z < 0.06$) and were observed for more than 35ks.

3.2. Temperature maps

Ideally, one would prefer to compute a temperature map using spatially resolved spectroscopy as we did in Laganá et al. (2008). This, however, is very timing consuming. We opt for another approach, namely to compute the hardness ratio maps and then convert them to temperature map. In this way, we are able to detect significant small-scale features without resorting to a computer intensive method.

The hardness ratio (HR) maps, or color maps, are defined as the ratio of the fluxes in two different bands and can be interpreted as a projected temperature map. They can be defined as [smoothed hard-energy band image - smoothed soft-energy band image] / [smoothed hard-

¹ <http://cxc.harvard.edu/ciao3.4/threads/createL2/>

Table 1: Observational information

Cluster	RA (J2000)	Dec (J2000)	z	Detector	Exposure time (ks)	Soft band* (keV)	Hard band* (keV)	n_{H}^{\ddagger} (10^{20} cm^{-2})
Abell 85	00:41:37.80	-09:20:33.0	0.055	ACIS-I	38.91	0.3-1.4	1.4-6.0	2.78
Abell 426	03:19:48.20	+41:30:42.2	0.018	ACIS-S	98.20	0.3-1.4	1.4-6.0	13.6
Abell 496	04:33:37.00	-13:14:17.0	0.033	ACIS-S	76.08	0.3-1.3	1.3-6.0	3.78
Abell 3376	06:02:10.00	-39:57:21.0	0.046	ACIS-I	44.85	0.3-1.5	1.5-6.0	4.58
Abell 754	09:09:09.00	-09:39:39.0	0.054	ACIS-I	44.77	0.3-1.5	1.5-6.0	4.82
Hydra A	09:18:05.70	-12:05:42.5	0.013	ACIS-S	100.13	0.3-1.2	1.2-6.0	4.60
Centaurus	12:48:48.90	-41:18:44.4	0.011	ACIS-S	90.19	0.3-1.2	1.2-6.0	8.56
Abell 1644	12:57:33.00	-17:20:28.0	0.047	ACIS-I	52.17	0.3-1.6	1.6-6.0	4.11
Abell 1991	14:54:31.50	+18:38:32.0	0.059	ACIS-S	38.81	0.3-1.1	1.1-6.0	2.46
Abell 2052	15:16:44.50	+07:01:16.6	0.035	ACIS-S	128.63	0.3-1.2	1.2-6.0	2.71
Abell 2107	15:39:39.00	+21:46:58.0	0.041	ACIS-I	36.04	0.3-1.5	1.5-6.0	4.45
Ophiuchus	17:12:27.80	-23:22:11.5	0.028	ACIS-S	51.18	1.3-4.0	4.0-7.0	40.0
Abell 3667	20:13:07.25	-56:53:24.0	0.056	ACIS-I	105.01	0.3-1.6	1.6-6.0	4.44
Abell 4059	23:57:00.70	-34:45:33.0	0.047	ACIS-S	93.34	0.3-1.2	1.2-6.0	1.21
Abell 2589	23:23:57.40	+16:46:39.0	0.041	ACIS-S	54.13	0.3-1.3	1.3-6.0	3.15

* Soft and hard bands used to construct the hardness ratio.

‡ Hydrogen column densities adopted to construct HR (Dickey & Lockman 1990).

energy band image + smoothed soft-energy band image]. These bands are specified for each cluster in Table 1 and were chosen such that the two bands had almost identical net counts.

We used the *csmooth* tool in *Chandra* Interactive Analysis of Observations (CIAO), an adaptive smoothing algorithm, to bin the data using bins of large angular size in order to examine possible structures in the image. In adaptive binning, the size of the smoothing kernel changes over the original image to create a constant S/N per pixel in the output image. The hard and soft energy band images were smoothed identically, with the same adaptive kernel, avoiding spurious artifacts and yielding meaningful hardness ratios.

To convert the HR maps into temperature maps, we required a simple algorithm to compare the relative fluxes in different X-ray bands with a theoretical plasma emission model. Thus, based on the assumption of a single temperature, the HR- kT relation was estimated for each cluster, and an example is shown in Fig. 1 for A496. Watanabe et al. (2001) also used this procedure to construct the temperature map of Ophiuchus using ASCA data. To do so, we took into account the weighted response matrices (RMFs), affective area files (ARFs) generated with CIAO 3.4., exposure maps of each observation, the hydrogen column densities of each cluster (as specified in Table 2), and adopted a fixed metallicity value of 0.35 for all clusters. In Fig. 1, we show that the HR conversion into plasma temperature exhibits little variation assuming different metallicity values.

4. Results

In Fig.2, we present the X-ray images, temperature and substructure maps of the 15 clusters in our sample. To investigate the properties of these clusters, we also present in

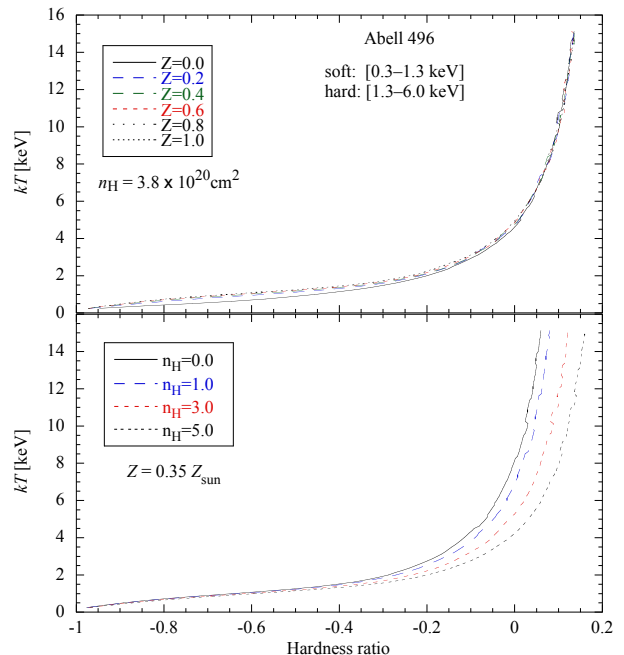


Fig. 1: Hardness ratio conversion into plasma temperature, using Abell 496 as an example. **Top:** HR-to-temperature conversion assuming different metallicity values (in solar units) when all other parameters remained fixed. **Bottom:** HR-to-temperature conversion assuming different hydrogen column densities (in 10^{20} cm^{-2}). While a metallicity error has an insignificant effect, n_{H} is important for an accurate determination of kT (in particular at high temperatures).

Tab.2 the mean X-ray temperature, the cooling-flow time, and the X-ray luminosity obtained from the literature.

Although not clearly evident in all temperature maps, a spiral-like structure in the inner part of 7 clusters (A85,

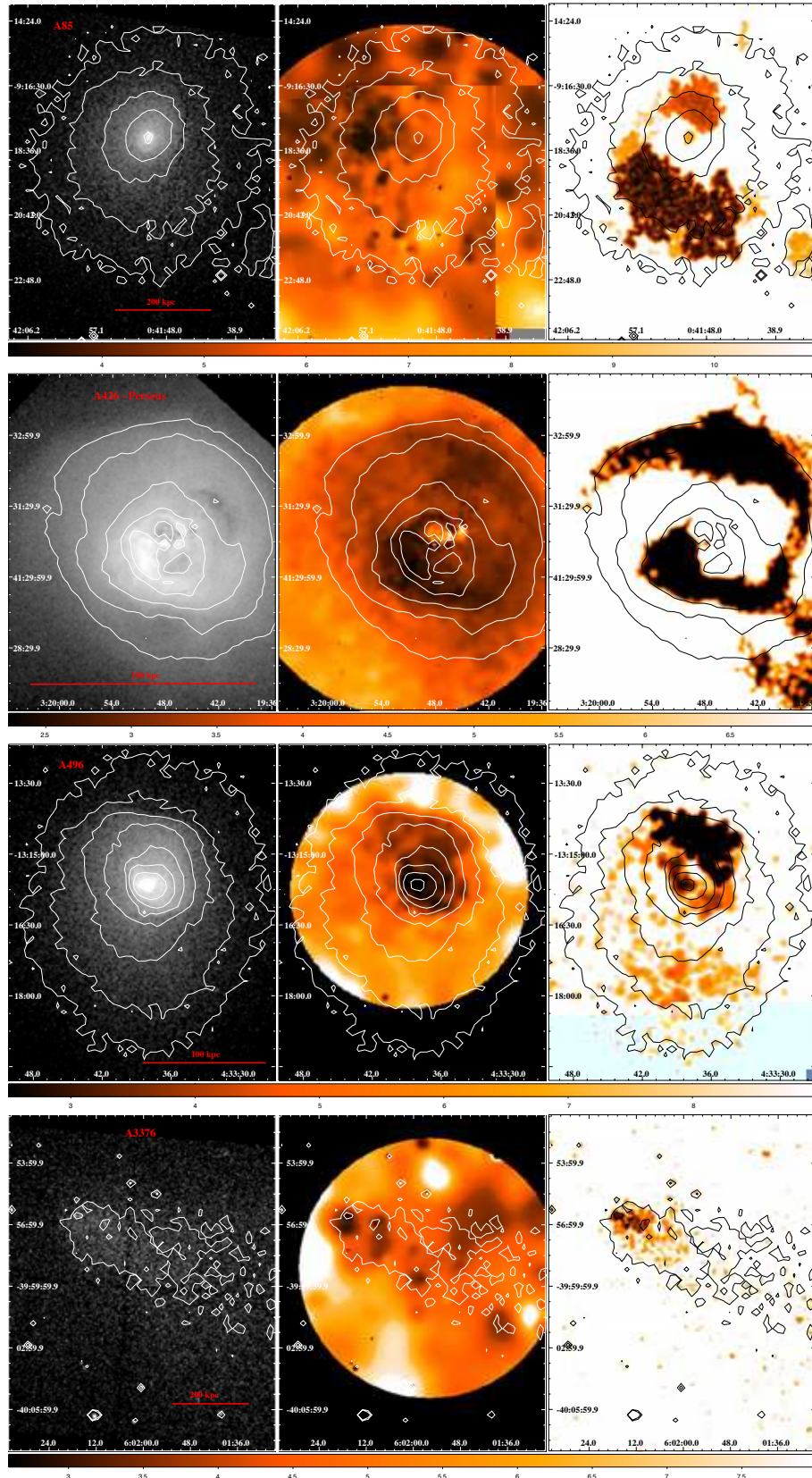


Fig. 2: Left panels: X-ray image; middle panel: temperature maps; and right panels: substructure maps for A85, A426 (Perseus), A496, and A3376. The color-bar indicates the temperature in keV.

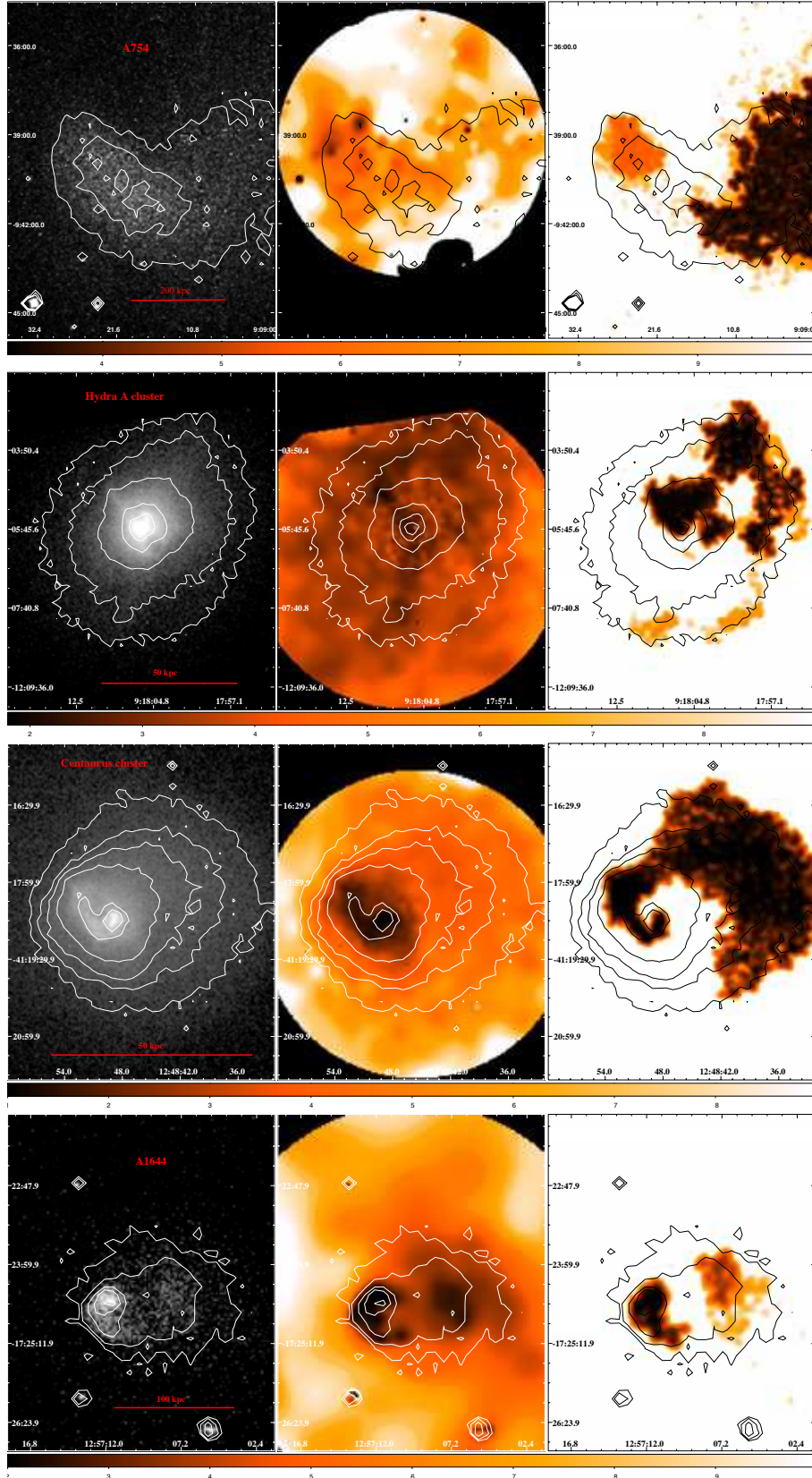


Fig. 2: *Cont.* Left panels: X-ray image; middle panel: temperature maps; and right panels: substructure maps for A754, Hydra A cluster, Centaurus cluster, and A1644. The color-bar indicates the temperature in keV.

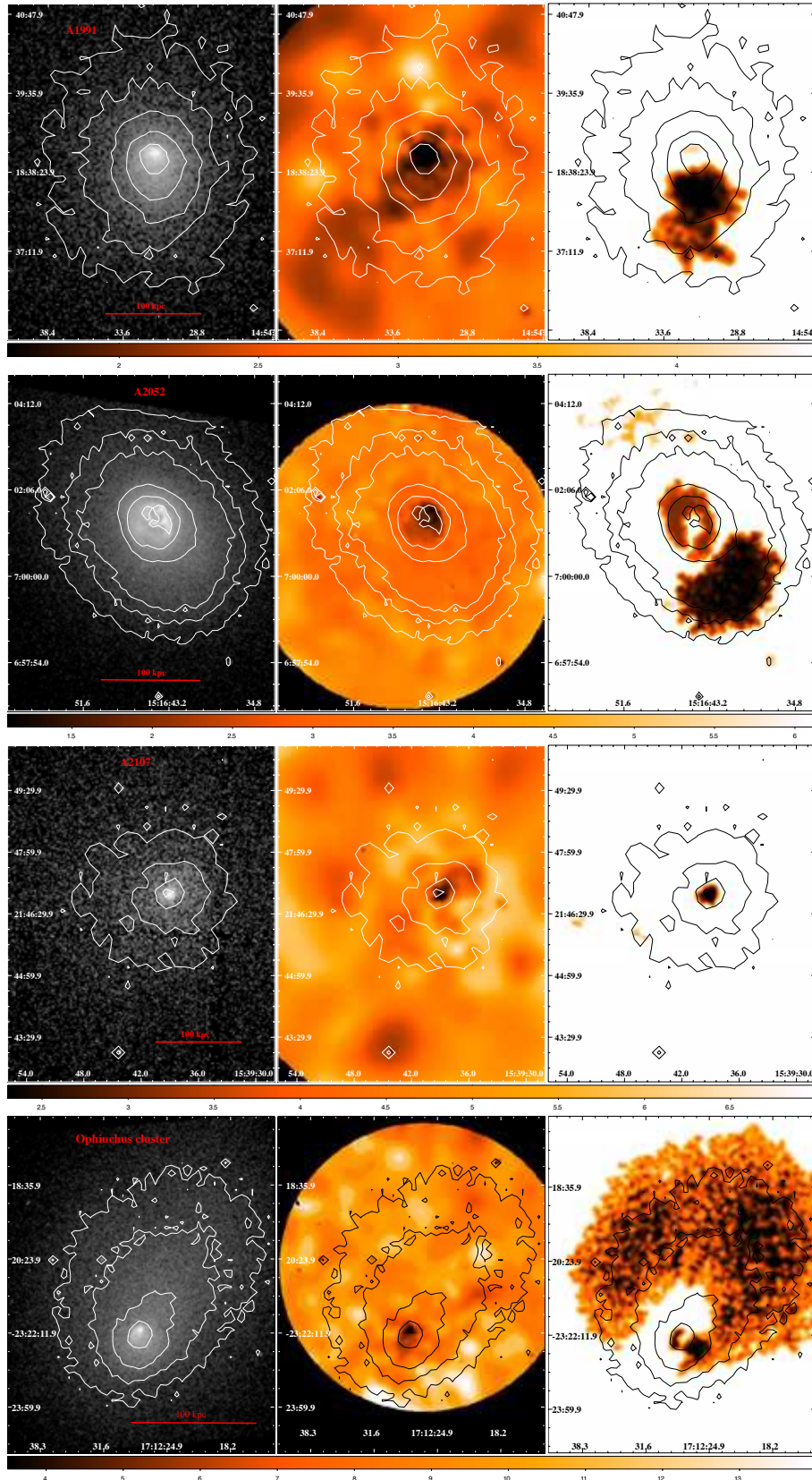


Fig. 2: *Cont.* Left panels: X-ray image; middle panel: temperature maps; and right panels: substructure maps for A1991, A2052, A2107, and Ophiuchus cluster. The color-bar indicates the temperature in keV.

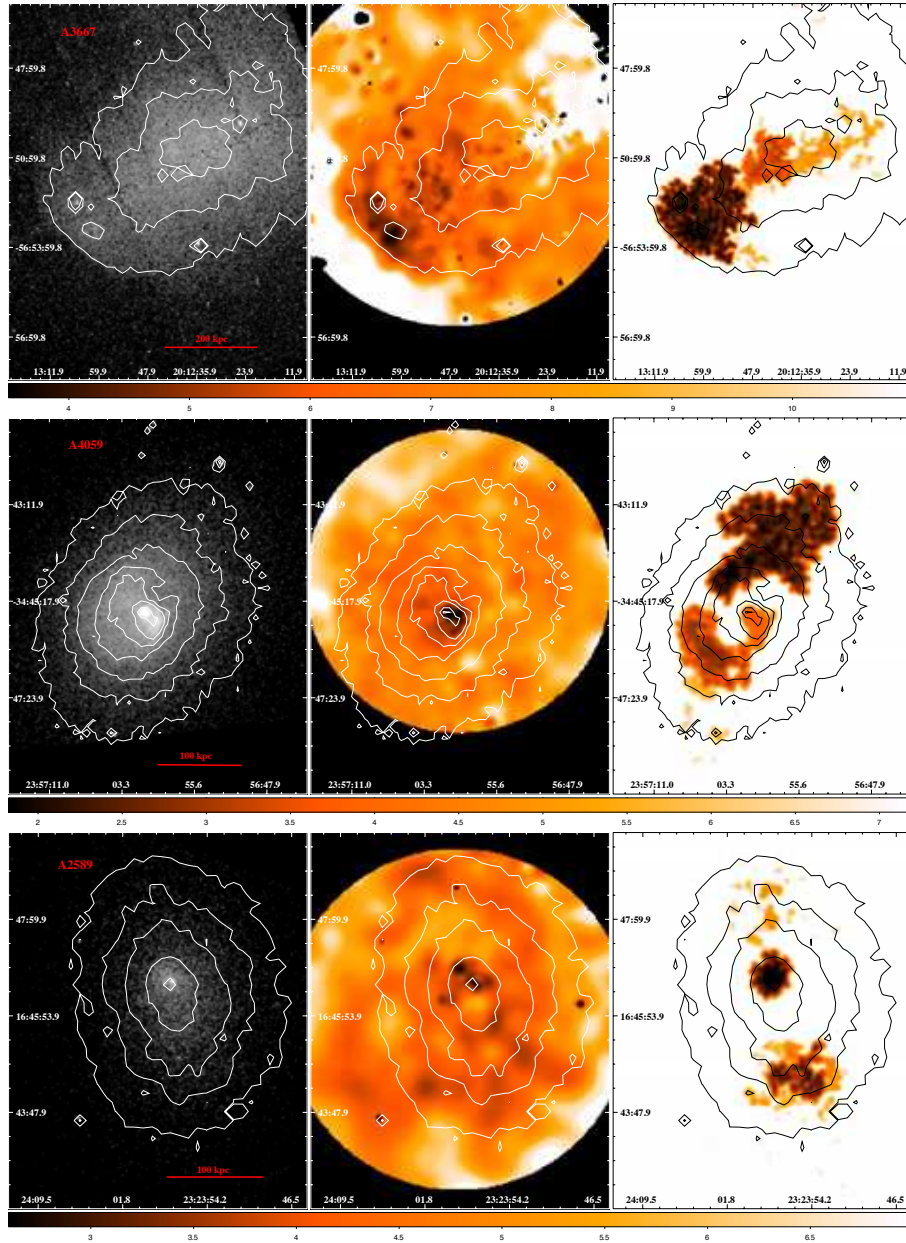


Fig. 2: *Cont.* Left panels: X-ray image; middle panel: temperature maps; and right panels: substructure maps for A3667, A4059, and A2589. The color-bar indicates the temperature in keV.

A426, A496, Hydra A cluster, Centaurus, Ophiuchus, and A4059) is detected in the substructure maps. These clusters are those of the highest cooling-flow rate and most are known to have a strong radio galaxy at the centre.

Since the variations in temperature and density inside shocks are positive correlated, that these patterns are also regions of low temperature and high density argues against strong shocks. These substructures instead, resemble the edges of cold fronts found in several clusters (e.g., Markevitch & Vikhlinin 2007; Dupke et al. 2007). Cold fronts can be directly related to cluster merging activities, and by comparing our results with numerical simulations (Gómez et al. 2002; Ascasibar & Markevitch 2006) one can see that the spiral-like features found here

are morphologically similar to those found in their simulations. This indicates that their nature is probably dynamical and a possible scenario for its formation is discussed in Sect. 5.

Here, we provide additional information about each cluster in the sample, by highlighting key aspects of previous studies.

4.1. Abell 85

This is a well-known subclump cluster that has a cold-front (Kempner et al. 2002) and is a merger candidate. The optical properties of this cluster are indicative of evidence for galaxy star formation in the filament be-

Table 2: Cluster properties

Cluster	K. Arnaud [†]		Chen et al. (2007) [†]			Ikebe et al. (2002) [†]		Edge et al. (1992) [†]	
	kT (keV)	M ($M_{\odot} \text{ yr}^{-1}$)	kT (keV)	M ($M_{\odot} \text{ yr}^{-1}$)	L_X [0.1 – 2.4keV] ($h_{70}^{-2} 10^{44} \text{ erg/s}$)	kT (keV)	L_X [0.1 – 2.4keV] ($h_{70}^{-2} 10^{44} \text{ erg/s}$)	L_X [2 – 10keV] ($h_{70}^{-2} 10^{44} \text{ erg/s}$)	M ($M_{\odot} \text{ yr}^{-1}$)
Abell 85	6.8	128.5	$6.10^{+0.20}_{-0.20}$	200^{+33}_{-27}	13.54 ± 0.15	$6.51^{+0.16}_{-0.23}$	1.81 ± 0.02	10.56	236
Perseus (A426)	6.4	94.9	$6.79^{+0.12}_{-0.12}$	481^{+31}_{-32}	–	$6.42^{+0.06}_{-0.06}$	2.93 ± 0.04	15.40	183
Abell 496	5.7	100.7	$4.13^{+0.08}_{-0.08}$	114^{+35}_{-28}	5.28 ± 0.07	$4.59^{+0.10}_{-0.10}$	0.69 ± 0.01	3.56	112
Abell 3376	–	–	$4.30^{+0.60}_{-0.60}$	0^{+0}_{-0}	3.02 ± 0.07	$4.43^{+0.39}_{-0.38}$	0.74 ± 0.02	–	–
Abell 754	–	–	$9.00^{+0.50}_{-0.50}$	0^{+0}_{-0}	5.56 ± 0.15	$9.00^{+0.35}_{-0.34}$	4.0 ± 0.10	14.70	24
Hydra A	–	–	$3.80^{+0.20}_{-0.20}$	293^{+50}_{-84}	8.18 ± 0.06	–	–	3.89	315
Centaurus	2.3	31.3	$3.68^{+0.06}_{-0.06}$	24^{+6}_{-5}	1.67 ± 0.06	–	–	0.81	18
Abell 1644	5.1	19.3	$4.70^{+0.90}_{-0.70}$	0^{+0}_{-0}	5.49 ± 0.48	$4.70^{+0.90}_{-0.70}$	0.73 ± 0.06	3.33	19
Abell 1991	4.6	71.0	–	–	–	–	–	–	–
Abell 2052	3.7	30.8	$3.03^{+0.04}_{-0.04}$	108^{+188}_{-49}	3.32 ± 0.06	$3.12^{+0.10}_{-0.09}$	0.43 ± 0.01	1.97	90
Abell 2107	6.5	0.0	–	–	–	–	–	–	–
Ophiuchus	–	–	$10.26^{+0.32}_{-0.32}$	0^{+0}_{-0}	–	$10.25^{+0.30}_{-0.36}$	2.2 ± 0.07	21.28	75
Abell 3667	–	–	$7^{+0.60}_{-0.60}$	0^{+0}_{-0}	13.27 ± 0.15	$6.28^{+0.27}_{-0.26}$	1.78 ± 0.02	11.59	0
Abell 4059	–	–	$4.10^{+0.30}_{-0.30}$	69^{+20}_{-15}	3.92 ± 0.08	$3.94^{+0.15}_{-0.15}$	0.52 ± 0.01	2.65	124
Abell 2589	–	–	$3.70^{+2.20}_{-1.10}$	19^{+53}_{-19}	2.62 ± 0.06	$3.38^{+0.13}_{-0.13}$	3.44 ± 0.08	–	–

[†] All values were converted to a common cosmology with a Hubble constant given as $H_0 = 70 \text{ km s}^{-1} \text{ Mpc}^{-1}$.

tween the main cluster and the subclump (Boué et al. 2008), which is consistent with the previous hypothesis that the X-ray filament in Abell 85 is a gravitationally bound structure consisting of groups falling into the main cluster (Lima Neto et al. 2001; Durret et al. 2003).

We clearly see a spiral-like structure in the substructure map. However, no corresponding structure appears in the temperature map.

4.2. Abell 426 - Perseus

Churazov et al. (2003) presented XMM-Newton data in which a spiral-like structure was detected in temperature and surface brightness maps. These authors concluded that this feature is possibly a contact discontinuity separating the main cluster gas from the gas of the infalling subcluster. A chain of galaxies is also associated with this region, probably tracing the filament along which the merger started.

Since it has a strong central radio galaxy, NGC 1275, Boehringer et al. (1993) argued that the thermal plasma was displaced by the inner parts of the radio lobe. Fabian et al. (2002) examined in detail the interaction between the radio source 3C84 and the surrounding medium, arguing that the inner lobes are currently expanding subsonically.

From our results, one can see that this cluster is one with the most prominent spiral-arm patterns in both temperature and substructure maps. The substructure found here is almost identical to that detected by Churazov et al. (2003) (see their Fig. 7).

4.3. Abell 496

This cluster hosts a prominent cold-front (Dupke & White 2003), which is a sign of a recent minor merger, and although its report has not received much attention,

a very prominent spiral-like pattern was detected by Laganá et al. (2008) in XMM-Newton data.

In Fig. 2, a spiral-like feature is evident in both the substructure and temperature map. The pattern that appears in the temperature map is very similar in form to that of A85.

4.4. Abell 3376

This is a nearby ongoing merger cluster that was observed by both *Suzaku* (Kawano et al. 2008) and XMM-Newton (Bagchi et al. 2006). A non-thermal radio-emitting structure at the outskirts of this cluster was identified by the latter authors. They suggested that this structure probably traces the elusive shocks of cosmological large-scale matter flows.

4.5. Abell 754

A754 was one of the first clusters for which an X-ray temperature map was derived from ROSAT (Henry & Briel 1995) and ASCA (Henriksen & Markevitch 1996) data, in which the gas velocity map (Evrard et al. 1996) indicated a plume-like pattern. A *Chandra* data analysis infer a more complex merger geometry, possibly involving more than two subclusters (Markevitch et al. 2003). From XMM-Newton data, Kassim et al. (2001) and Bacchi et al. (2003) confirmed that this cluster is a major-merger cluster and also detected a plume-like feature at its centre. There is a diffuse radio source associated with this cluster (Henry et al. 2004).

In this work, a large substructure is detected but does not exhibit any particular shape.

4.6. A780 - Hydra A cluster

Fitchett & Merritt (1988) examined the dynamics of the Hydra cluster find that the velocity distribution of galaxies

close the cluster centre is very flat. Although they did not propose an infalling group scenario, they did consider the importance of substructures in this cluster,

Chandra observations of the Hydra cluster detect a feature in the X-ray surface brightness surrounding radio lobes of the active galactic nucleus (AGN) at the cluster centre (Nulsen et al. 2005). These authors proposed that the shock front is driven by the expanding radio lobes in addition to the “new structure on smaller scales” is associated with the radio source. Wise et al. (2007) confirmed that the complex system found in this cluster was created by a continuous outflow or a series of bursts in the nucleus of the central galaxy. In this particular case, a merger has not been mentioned in the literature as a possible mean of forming this substructure.

In this work, we were able to detect a truncated spiral-like feature in the substructure map that has a corresponding structure of relatively low temperature.

4.7. Centaurus

To explain the particular morphology of this cluster, Churazov et al. (1999) analysed ASCA imaging and spectral results, and proposed that there is a subcluster centred on NGC 4709 that is merging with the main cluster centred on NGC 4696.

Sanders & Fabian (2006) performed a detailed analysis of the core of the Centaurus cluster using a *Chandra* deep X-ray observation and XMM-Newton data. To explain the high metallicity present in the core of this cluster, the authors proposed a model in which the inner core of the Centaurus cluster has not experienced a major disruption within the past 8 Gyr, or even longer. In their temperature map, the plume-like feature is evident, this finding then attracted little attention. They also reported the discovery of ripple-like X-ray surface brightness oscillations in the core of this cluster of galaxies, which they asserted were indicative of sound waves generated by the repeated inflation of central radio bubbles.

From Fig. 2, one can see that this cluster has one of the most prominent spiral-like features detected in a substructure map. The very inner region of this enormous structure is also associated with a region of relatively low temperature in the temperature map.

4.8. Abell 1644

This is a complex merging system that was observed with XMM-Newton, and found to consist of a main cluster and a subcluster (Reiprich et al. 2004). These authors also detected a trail of cool, metal-rich gas closer to the subcluster. The combination of X-ray, optical, and radio data results imply that the subcluster has passed by the main cluster off-axis. Although temperature maps were presented in their work, the plume-like feature was not resolved by XMM-Newton.

In our analysis, a discontinuous spiral-like feature is present in the substructure map. This pattern is not as clearly evident as in Centaurus, Perseus, and A85 but it does resemble these structures. Unfortunately, only the inner part of the substructure has a corresponding feature in the temperature map.

4.9. Abell 1991

Sharma et al. (2004) analysed XMM-Newton data and detected an asymmetric surface brightness distribution with respect to the central galaxy. These authors detected bright knots of soft X-ray emission embedded in a cometary structure located north of the optical centre of the cD galaxy. According to these authors, the knots have no obvious association with the radio source.

4.10. Abell 2052

Zhao et al. (1993) reported a VLA detection of a radio source at the core of this cluster. Blanton et al. (2003, 2009) carried out a *Chandra* X-ray data analysis of the large-scale properties of the cluster as well as the central region (which contains a radio source) presenting temperature and abundance profiles.

Two clear substructures are present in Fig.2 but they do not resemble to the other spiral-like feature presented in this work.

4.11. Abell 2107

Fujita et al. (2006) presented an analysis of *Chandra* observation of this cluster. Since the cD galaxy has a large peculiar velocity and the ICM in the central region has an irregular structure, these authors concluded that this cluster is undergoing a merger.

From our results, A2107 contains the smallest substructure and has almost symmetric X-ray contours providing no evidence of a recent merger.

4.12. Ophiuchus

Ophiuchus is one of the hottest X-ray cluster and is located 12 deg from the Galactic centre (Fujita et al. 2008). Using ASCA data, Matsuzawa et al. (1996) acquired images in the energy range of 0.7-10 keV that indicated that the peak of the X-ray surface brightness is coincident with the cD galaxy. Watanabe et al. (2001) presented temperature and metallicity profiles obtained with ASCA data, which contained no evidence of a plume-like feature. In their analysis, the ROSAT archival data inferred an ongoing merger, but a *Chandra* image indicates that this cluster has a cool-core that remains undisturbed. Thus, if there is an ongoing merger, it must be a minor merger (e.g., Watanabe et al. 2001).

From the results presented in Fig.2, Ophiuchus is the cluster that has the most prominent spiral-like pattern in

its substructure map. However, no significant feature was detected in its temperature map.

4.13. Abell 3667

This cluster has a double radio halo outside its central region (Rottgering et al. 1997; Markevitch et al. 1999). The galaxy distribution is bimodal (Proust et al. 1988), the main component being located around the cD galaxy. A multiwavelength study confirmed that it is probably a merger cluster based on *Chandra* and optical data (Owers et al. 2009a). Its X-ray image shows a clear cold front.

4.14. Abell 4059

Heinz et al. (2002) affirmed that there are clear signs of interaction between the radio galaxy and the ICM. However, these authors did not find any one-to-one spatial correspondence between the radio lobes and the X-ray cavities (Heinz et al. 2002). Huang & Sarazin (1998) argued that it is likely that the radio plasma from the cD galaxy may have displaced the X-ray gas and created the X-ray cavities.

On the other hand, Choi et al. (2004) analysed various scenarios concluding that the most probable is that of a compression front associated with ICM bulk motion.

Reynolds et al. (2008) analysed a *Chandra* deep observation, detect a subtle discontinuity in the gradient of the surface brightness that is approximately semi-circular in form and centred on the radio galaxy. The previous *Chandra* observations reported by Heinz et al. (2002) and Choi et al. (2004) were of insufficient signal-to-noise ratio to detect this feature. Although it cannot be rigorously proven, Reynolds et al. (2008) interpreted this feature as a weak shock caused by the radio galaxy activity. Similar shocks are seen in all hydrodynamic simulations of jet/ICM interactions (Heinz et al. 2002; Vernaleo & Reynolds 2006, e.g.).

In this work, we have shown that this cluster also has a spiral-like substructure. The inner part of this pattern is related to a region of lower temperature, as it can be seen in the temperature map of Fig.2.

4.15. Abell 2589

The hot gas in the core region of A2589 is undisturbed by interactions with a central radio source (Buote & Lewis 2004). Except for a 16 kpc shift in its X-ray centre, A2589 has a remarkably symmetrical X-ray image (Zappacosta et al. 2006).

5. Discussion

The literature contains detailed studies of large numbers of clusters with high cooling rates and a powerful radio galaxy, e.g., Hydra A (McNamara et al. 2000; David et al. 2001), Perseus (Fabian et al. 2000; Churazov et al. 2003),

and the Centaurus cluster (Taylor et al. 1994). There is a correlation between the radio emission by the central galaxies and the presence of a cooling-flow that has been known since Burns et al. (1981) and Jones & Forman (1984). The cooling gas is driven towards a massive object in the central galaxy that might produce the radio emission. However, what is quite surprising is that clusters exhibiting distinctive spiral-like structures are those with the greatest cooling-flows (see Table 2) and containing a powerful radio galaxy. The only exception is A2052 that contains an AGN (Blanton et al. 2003, 2009) and does not exhibit a spiral-like substructure.

The presence of a strong cooling-flow and a powerful central radio galaxy indicates that its radiation has not yet had time to heat the surrounding gas of the inner parts of the clusters. This can be understood if we consider a cycle in which the cool gas feeds the central AGN that begins to heat the surrounding gas. While the central gas is not sufficiently heated and the cooling flow is not suppressed, there will be a stage where both the AGN and the cool gas will coexist.

The radio morphology of some clusters that exhibit spiral-like patterns appears quite different from most radio galaxies because they fill the X-ray cavities (regions of low density). Taylor et al. (2002) showed that the eastern lobe of the central radio galaxy of Centaurus cluster appears to fill the region bounded by the spiral-like structure, while the western lobes turns around it. Similar confinement has been found for other radio galaxies embedded in dense ICM. For example, radio emission filling X-ray cavities was found at the core of Perseus cluster (Boehringer et al. 1993; Fabian et al. 2000, 2002), A2029 (Taylor et al. 1994), and Hydra A cluster (A780) (McNamara et al. 2000).

The ICM of merging clusters exhibit a variety of signatures of mergers such as cold-fronts and bow shocks. Although the most prominent cold fronts are produced in major mergers, cold fronts produced by minor mergers are expected to be far more frequent. Minor mergers generate subsonic turbulent gas motions within the cluster without destroying the cool-core. Different morphological features can be created by of minor mergers, such as comet-like tails, bridges, plumes, and edges (Poole et al. 2006). Thus, one possibility for the origin of the spiral structure found in 7 clusters of our sample is that they are the signature of a small galaxy cluster or group minor merger with a more massive cluster.

In a high-resolution numerical simulation of idealized cluster mergers, Ascasibar & Markevitch (2006) concluded that if an infalling subcluster has a non-zero impact parameter, the cool gas of the main cluster acquires angular momentum, producing in a spiral-like feature of cold front due to the gas sloshing. In their simulation, after 1.9 Gyr (see their Fig. 7) one can discern a spiral-like pattern in both the gas density and temperature distribution, that are morphologically similar to the structure found here. Since they used a mass ratio of 1:5, the cooling core is preserved.

The numerical simulations of Gómez et al. (2002) also reproduce the results found here. In their merger 7, the subcluster has a small gas fraction and they assume a mass ratio of 1:16 so that the cooling-flow is not disrupted during the merger. An alternative explanation of the spiral-like structure is a contact discontinuity separating the main cluster gas from the gas of the infalling subcluster. However, it is also possible that the gas is stripped away from the infalling subcluster far from the core, never reaching the inner region of the main cluster (Churazov et al. 2003). In this way, the observed structure consists only of the disturbed gas of the main cluster. A metallicity analysis would be able to distinguish between the above scenarios. If the cold gas in the spiral-like pattern is caused by the main cluster gas sloshing, the metallicity in this region should be equal to the metallicity in the inner part of the main cluster. On the other hand, if it is a gas discontinuity, the metallicity in the spiral arm would be different from the inner part of the main cluster. The ICM enrichment analysis for this sample will be presented in a forthcoming work.

In minor merger scenario, it is more likely that the cooling flow continues to feed the central galaxy. The radio emission then, permeates the regions of low density, that is, fills the X-ray cavities because it is confined by the spiral-like feature. The ICM acts to distort the radio emission producing the radio morphologies, as can be seen in some clusters.

We note that the detection of spiral-like features is not limited to the clusters in our sample but has also been achieved in other clusters, such as A1975 (Fabian et al. 2001), A262 (Blanton et al. 2004), A2029 (Clarke et al. 2004), A5098 (Randall et al. 2009), A1795 (Liuzzo et al. 2009), and A1201 (Owers et al. 2009b). This kind of pattern has also been observed in galaxy groups (Gastaldello et al. 2007; Randall et al. 2009), indicating that they are not restricted to clusters.

Since we find that a high number of clusters contain these structures, it would be interesting to bolster these findings by using numerical simulations. In particular, it would be instructive to study the frequency of off-axis merger halos, as a function of redshift, that produce a cool gas spiral-like pattern when adopting mass ratios of 1:5 (Ascasibar & Markevitch 2006) and 1:16 (Gómez et al. 2002). Unfortunately, these studies are beyond the scope of our present investigation.

From the theoretical point of view, future numerical hydrodynamical simulations could detect the signatures of cluster mergers that could then be compared with observations. In this sense, statistical studies of cluster morphology and substructures would provide important constraints on models of structure formation and the evolution of the observed cluster properties. Despite the large amount of available data, the dynamical evolution of ICM substructures remains poorly understood. Here we have studied in detail 15 nearby galaxy clusters highlighting the incidences of a particular ICM substructure morphology.

6. Synthetic image

We now present a synthetic image, created using the *cfit-sio* routine (a library of routines for reading and writing data files in the FITS data format). This synthetic image was constructed by adding multiple components to roughly mimic the Perseus cluster X-ray surface brightness. The synthetic image was the result of adding a 2D β -model, an exponential spiral pattern, and two bubbles in the inner region of the cluster. The components and the result of their addition is seen in Fig. 3.

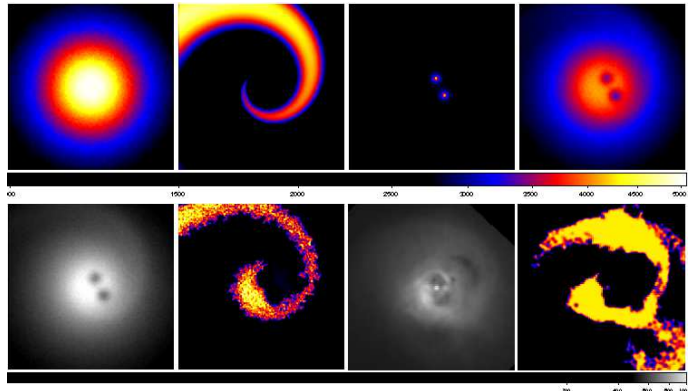


Fig. 3: Synthetic image constructed to roughly reproduce the Perseus cluster X-ray surface brightness. Top panels from left to right: 2D β -model, exponential spiral pattern, two bubbles, and the sum of these three components. Bottom panels from left to right: X-ray synthetic surface brightness, substructure map from this previous image, Perseus X-ray surface brightness, and its substructure map.

The goal of generating this synthetic image is to follow the same procedures applied to true clusters, on determining substructure, and comparing with the substructure of the Perseus cluster. Although clearly present, one can see that the spiral pattern is not distinctive in the synthetic surface brightness image (see top panel of Fig. 3), which shows the importance of this method in finding structures that are hardly discernible by eye.

The synthetic-image substructure map shows the result obtained in a spiral-like pattern structure very similar to the one found in the Perseus clusters, reinforcing the detectability of these spiral-like patterns. Furthermore, the result shows that the Perseus cluster X-ray surface brightness and substructures can be described well by the addition of three components, to produce in particular an exponential spiral-like pattern, similar to that found in the results of numerical simulations performed by Ascasibar & Markevitch (2006).

7. Conclusions

In the most widely accepted scenario of structure formation, clusters of galaxies form hierarchically by means of

mergers. Besides the modification of galaxy distribution and triggering of star formation, these merger events produce variations in the physical properties, such as density and temperature variations that can be observed in X-rays. In this sense, the substructure maps have provided a powerful means of identifying hidden structures that are the last record of the merger history.

We have presented 7 (A85, A426, A496, Hydra A cluster, Centaurus, Ophiuchus and A4059) out of 15 clusters that exhibit for spiral-like substructure correlated spatially with the boundaries of cold-fronts and cavities. The cavities inside these patterns are, in most of cases, associated with radio emission. The aim of this study has been to determine the frequency of this morphological pattern at the centres of nearby clusters. Our analysis has shown how observational studies can improve the constraints on numerical simulations of structure formation and improve our understanding of ICM physical properties.

Comparing our results to numerical simulations (Ascasibar & Markevitch 2006), we have discussed the suitability of a model in which this spiral-like pattern is produced by an off-axis minor-merger that displaces the central cool gas. Since the minor merger does not disrupt the cool core, the central cool gas is still driven towards the central object that may produce the radio emission. This radio emission is bounded by the ICM inhomogeneities that will probably create an overall radio appearance that is quite different from most radio galaxies. Thus, we suggest that these distorted radio-emission morphologies may be caused by the confinement of dense X-ray gas in the spiral pattern. However, our interpretation of the spiral-like pattern and its relation to X-ray cavities and radio emission should be tested by additional more sophisticated simulations that ascertain possible merger signatures.

Acknowledgements. The authors thank Florence Durret that triggered this work. The authors thank the anonymous referee for useful suggestions. The authors also acknowledge financial support from the Brazilian agencies FAPESP (grants: 2006/56213-9, 2008/04318-7, and 2008/05970-0) and CNPq (grant: 472012/07-0).

References

- Ascasibar, Y. & Markevitch, M. 2006, *ApJ*, 650, 102
- Bacchi, M., Feretti, L., Giovannini, G., & Govoni, F. 2003, *A&A*, 400, 465
- Bagchi, J., Durret, F., Neto, G. B. L., & Paul, S. 2006, *Science*, 314, 791
- Blanton, E. L., Randall, S. W., Douglass, E. M., et al. 2009, *ApJ*, 697, L95
- Blanton, E. L., Sarazin, C. L., & McNamara, B. R. 2003, *ApJ*, 585, 227
- Blanton, E. L., Sarazin, C. L., McNamara, B. R., & Clarke, T. E. 2004, *ApJ*, 612, 817
- Boehringer, H., Voges, W., Fabian, A. C., Edge, A. C., & Neumann, D. M. 1993, *MNRAS*, 264, L25
- Boué, G., Durret, F., Adami, C., et al. 2008, *A&A*, 489, 11
- Brüggen, M. & Kaiser, C. R. 2002, *Nature*, 418, 301
- Buote, D. A. & Lewis, A. D. 2004, *ApJ*, 604, 116
- Burns, J. O. 1990, *AJ*, 99, 14
- Burns, J. O., White, R. A., & Haynes, M. P. 1981, *AJ*, 86, 1120
- Chen, Y., Reiprich, T. H., Böhringer, H., Ikebe, Y., & Zhang, Y.-Y. 2007, *A&A*, 466, 805
- Choi, Y.-Y., Reynolds, C. S., Heinz, S., et al. 2004, *ApJ*, 606, 185
- Churazov, E., Brüggen, M., Kaiser, C. R., Böhringer, H., & Forman, W. 2001, *ApJ*, 554, 261
- Churazov, E., Forman, W., Jones, C., & Böhringer, H. 2003, *ApJ*, 590, 225
- Churazov, E., Gilfanov, M., Forman, W., & Jones, C. 1999, *ApJ*, 520, 105
- Clarke, T. E., Blanton, E. L., & Sarazin, C. L. 2004, *ApJ*, 616, 178
- David, L. P., Nulsen, P. E. J., McNamara, B. R., et al. 2001, *ApJ*, 557, 546
- Dickey, J. M. & Lockman, F. J. 1990, *ARA&A*, 28, 215
- Dupke, R. & White, III, R. E. 2003, *ApJ*, 583, L13
- Dupke, R., White, III, R. E., & Bregman, J. N. 2007, *ApJ*, 671, 181
- Durret, F. & Lima Neto, G. B. 2008, *Advances in Space Research*, 42, 578
- Durret, F., Lima Neto, G. B., Forman, W., & Churazov, E. 2003, *A&A*, 403, L29
- Edge, A. C., Stewart, G. C., & Fabian, A. C. 1992, *MNRAS*, 258, 177
- Eilek, J. A. 2004, in *The Riddle of Cooling Flows in Galaxies and Clusters of galaxies*, ed. T. Reiprich, J. Kempner, & N. Soker, 165
- Evrard, A. E., Metzler, C. A., & Navarro, J. F. 1996, *ApJ*, 469, 494
- Fabian, A. C., Celotti, A., Blundell, K. M., Kassim, N. E., & Perley, R. A. 2002, *MNRAS*, 331, 369
- Fabian, A. C., Sanders, J. S., Ettori, S., et al. 2001, *MNRAS*, 321, L33
- Fabian, A. C., Sanders, J. S., Ettori, S., et al. 2000, *MNRAS*, 318, L65
- Finoguenov, A., Böhringer, H., & Zhang, Y.-Y. 2005, *A&A*, 442, 827
- Fitchett, M. & Merritt, D. 1988, *ApJ*, 335, 18
- Fujita, Y., Hayashida, K., Nagai, M., et al. 2008, *PASJ*, 60, 1133
- Fujita, Y., Sarazin, C. L., & Sivakoff, G. R. 2006, *PASJ*, 58, 131
- Gastaldello, F., Buote, D. A., Humphrey, P. J., et al. 2007, *ApJ*, 669, 158
- Gómez, P. L., Loken, C., Roettiger, K., & Burns, J. O. 2002, *ApJ*, 569, 122
- Heinz, S., Choi, Y.-Y., Reynolds, C. S., & Begelman, M. C. 2002, *ApJ*, 569, L79
- Heinz, S., Reynolds, C. S., & Begelman, M. C. 1998, *ApJ*, 501, 126
- Henriksen, M. J. & Markevitch, M. L. 1996, *ApJ*, 466, L79
- Henry, J. P. & Briel, U. G. 1995, *ApJ*, 443, L9
- Henry, J. P., Finoguenov, A., & Briel, U. G. 2004, *ApJ*, 615, 181
- Huang, Z. & Sarazin, C. L. 1998, *ApJ*, 496, 728
- Ikebe, Y., Reiprich, T. H., Böhringer, H., Tanaka, Y., & Kitayama, T. 2002, *A&A*, 383, 773
- Jones, C. & Forman, W. 1984, *ApJ*, 276, 38
- Kassim, N. E., Clarke, T. E., Enßlin, T. A., Cohen, A. S., & Neumann, D. M. 2001, *ApJ*, 559, 785
- Kawano, N., Fukazawa, Y., Nishino, S., et al. 2008, *ArXiv:0805.3582*
- Kempner, J. C., Sarazin, C. L., & Ricker, P. M. 2002, *ApJ*, 579, 236
- Laganá, T. F., Lima Neto, G. B., Andrade-Santos, F., & Cypriano, E. S. 2008, *A&A*, 485, 633
- Lima Neto, G. B., Pislar, V., & Bagchi, J. 2001, *A&A*, 368, 440
- Liuzzo, E., Giovannini, G., & Giroletti, M. 2009, *ArXiv:0903.0812*
- Markevitch, M., Mazzotta, P., Vikhlinin, A., et al. 2003, *ApJ*, 586, L19
- Markevitch, M., Sarazin, C. L., & Vikhlinin, A. 1999, *ApJ*, 521, 526
- Markevitch, M. & Vikhlinin, A. 2007, *Phys. Rep.*, 443, 1
- Matsuzawa, H., Matsuoka, M., Ikebe, Y., Mihara, T., & Yamashita, K. 1996, *PASJ*, 48, 565
- McNamara, B. R., Nulsen, P. E. J., Wise, M. W., et al. 2005, *Nature*, 433, 45
- McNamara, B. R., Wise, M., Nulsen, P. E. J., et al. 2000, *ApJ*, 534, L135
- Nulsen, P. E. J., McNamara, B. R., Wise, M. W., & David, L. P. 2005, *ApJ*, 628, 629
- Owers, M. S., Couch, W. J., & Nulsen, P. E. J. 2009a, *ApJ*, 693, 901
- Owers, M. S., Nulsen, P. E. J., Couch, W. J., Markevitch, M., & Poole, G. B. 2009b, *ApJ*, 692, 702
- Poole, G. B., Fardal, M. A., Babul, A., et al. 2006, *MNRAS*, 373, 881
- Proust, D., Mazure, A., Sodre, L., Capelato, H., & Lund, G. 1988, *A&AS*, 72, 415
- Randall, S. W., Jones, C., Markevitch, M., et al. 2009, *ArXiv:0904.0610*
- Reiprich, T. H., Sarazin, C. L., Kempner, J. C., & Tittley,

- E. 2004, *ApJ*, 608, 179
- Reynolds, C. S., Casper, E. A., & Heinz, S. 2008, *ApJ*, 679, 1181
- Reynolds, C. S., Heinz, S., & Begelman, M. C. 2001, *ApJ*, 549, L179
- Rottgering, H. J. A., Wieringa, M. H., Hunstead, R. W., & Ekers, R. D. 1997, *MNRAS*, 290, 577
- Sanders, J. S. & Fabian, A. C. 2006, *MNRAS*, 371, 1483
- Sanders, J. S. & Fabian, A. C. 2008, *MNRAS*, 390, L93
- Sharma, M., McNamara, B. R., Nulsen, P. E. J., et al. 2004, *ApJ*, 613, 180
- Taylor, G. B., Barton, E. J., & Ge, J. 1994, *AJ*, 107, 1942
- Taylor, G. B., Fabian, A. C., & Allen, S. W. 2002, *MNRAS*, 334, 769
- Vernaleo, J. C. & Reynolds, C. S. 2006, *ApJ*, 645, 83
- Watanabe, M., Yamashita, K., Furuzawa, A., Kunieda, H., & Tawara, Y. 2001, *PASJ*, 53, 605
- Wise, M. W., McNamara, B. R., Nulsen, P. E. J., Houck, J. C., & David, L. P. 2007, *ApJ*, 659, 1153
- Zappacosta, L., Buote, D. A., Gastaldello, F., et al. 2006, *ApJ*, 650, 777
- Zhao, J.-H., Sumi, D. M., Burns, J. O., & Duric, N. 1993, *ApJ*, 416, 51